Antimagnetic rotation in ^{108,110}In with tilted axis cranking relativistic mean-field approach *

Wu-Ji Sun(孙无忌) Hai-Dan Xu(徐海丹) Jian Li(李剑)[1)] Yong-Hao Liu(刘永好)
Ke-Yan Ma(马克岩) Dong Yang(杨东) Jing-Bing Lu(陆景彬) Ying-Jun Ma(马英君)
College of Physics, Jilin University, Changchun 130012, China

Abstract: Based on tilted axis cranking relativistic mean-field theory within point-coupling interaction PC-PK1, the rotational structure and the characteristic features of antimagnetic rotation for $\Delta I = 2$ bands in ^{108,110}In are studied. Tilted axis cranking relativistic mean-field calculations reproduce the experimental energy spectrum well and are in agreement with the experimental $I \sim \omega$ plot, although the calculated spin overestimates the experimental values. In addition, the two-shears-like mechanism in candidate antimagnetic rotation bands is clearly illustrated and the contributions from two-shears-like orbits, neutron (gd) orbits above $Z = 50$ shell and $Z = 50, N = 50$ core are investigated microscopically. The predicted B(E2), dynamic moment of inertia $\mathfrak{J}^{(2)}$, deformation parameters β and γ, and $\mathfrak{J}^{(2)}/B$(E2) ratios in tilted axis cranking relativistic mean-field calculations are discussed and the characteristic features of antimagnetic rotation for the bands before and after alignment are shown.

Keywords: antimagnetic rotation, ^{108,110}In, tilted axis cranking relativistic mean field theory

PACS: 21.10.Re, 21.60.Jz, 23.20.-g **DOI:** 10.1088/1674-1137/40/8/084101

1 Introduction

Similar to rotational bands observed in molecules, many nuclei have an energy spectrum with a pronounced rotational character and the study of nuclear rotation has been at the forefront of nuclear structure for several decades. In particular, antimagnetic rotation (AMR) [1–3] is an exotic rotational phenomenon observed in near-spherical or weakly-deformed nuclei with weak electric quadrupole (E2) transitions, as compared to the rotation built on states with substantial quadrupole deformation resulting in strong E2 transitions. In antimagnetic rotation, the relation of energy and angular momentum is characterized by the so-called "two-shears-like mechanism", i.e., by simultaneous closing of the two blades of protons and neutrons toward the total angular momentum vector.

To date, antimagnetic rotation has attracted a lot of attention. Most AMR bands have been observed in the $A \sim 110$ mass region, and several AMR bands has been confirmed in Cd and Pd isotopes from lifetime measurements, including ^{105}Cd [4],^{106}Cd [5], ^{107}Cd [6], ^{108}Cd [7, 8], ^{110}Cd [9], ^{101}Pd [10] and ^{104}Pd [11]. The other candidates include ^{100}Pd [12], ^{108,110}In [13], ^{112}In [14] and ^{144}Dy [15].

During the last two decades, covariant density functional theory (CDFT), including relativistic mean-field (RMF) framework with point-coupling or mesonic-exchange interaction [16–18], has been a great success in describing many nuclear properties microscopically [19–22]. Moreover, without any additional parameters, the rotation excitations can be described self-consistently with the tilted axis cranking relativistic mean-field (TAC-RMF) approach [2, 3]. The TAC-RMF model has been successfully used in describing magnetic rotation (MR) and AMR microscopically and self-consistently, such as the AMR bands in ^{105,110}Cd [23, 24] and ^{112}In [14], and also the MR bands in ^{58}Fe [25], ^{60}Ni [26], ^{84}Rb [27], ^{86}Sr [28], ^{86}Y [29], ^{113,114}In [30, 31], ^{142}Gd [32] and ^{198,199}Pb [33]. In the $A \sim 110$ mass region, the $\Delta I = 2$ bands in ^{108,110}In were observed with AMR characteristics and the corresponding configurations were also suggested early in 2001 in Ref. [13]. Thus, it is necessary to study the candidate AMR bands in ^{108,110}In within TAC-RMF theory.

2 Theory and numerical details

In the TAC-RMF theory, nuclei are characterized by the relativistic fields $S(\boldsymbol{r})$ and $V^{\mu}(\boldsymbol{r})$ in the Dirac equa-

Received 5 February 2016, Revised 7 April 2016
∗ Supported by National Natural Science Foundation of China (11205068, 11205069, 11405072, 11475072, 11547308) and China Postdoctoral Science Foundation (2012M520667)
1) E-mail: jianli@jlu.edu.cn

tion in the intrinsic frame rotating with a constant angular velocity vector $\boldsymbol{\Omega}$ as

$$[\boldsymbol{\alpha}\cdot(\boldsymbol{p}-\boldsymbol{V})+\beta(M+S)+V-\boldsymbol{\Omega}\cdot\hat{\boldsymbol{J}}]\psi_k=\epsilon_k\psi_k. \quad (1)$$

Here $\hat{\boldsymbol{J}}=\hat{\boldsymbol{L}}+\frac{1}{2}\hat{\boldsymbol{\Sigma}}$ is the total angular momentum of the nucleon spinors, ϵ_k represents the single-particle Routhians for nucleons, and the fields S and $V^{\mu}(V,\boldsymbol{V})$ are connected in a self-consistent way to the densities and current distributions, for details see Refs. [22, 32]. The iterative solution of the above equation yields single-particle energies, expectation values of three components $\langle\hat{\boldsymbol{J}}_i\rangle$ of the angular momentum, energy, quadrupole moments, B(M1) and B(E2) transition probabilities, etc. The magnitude of the angular velocity $\boldsymbol{\Omega}$ is connected to the total angular momentum quantum number, i.e., spin I, by the semiclassical relation $\langle\hat{\boldsymbol{J}}\rangle\cdot\langle\hat{\boldsymbol{J}}\rangle=I(I+1)$. Moreover, by taking into account the quantal corrections [34], I can be approximately calculated by the approximation $J=\sqrt{I(I+1)}\approx I+1/2$.

In the following, we use the point coupling Lagrangian PC-PK1 [35] to investigate the candidate AMR bands in ^{108}In and ^{110}In. The calculations are free of additional parameters, and the pairing correlations are neglected. The Dirac equation for the nucleons is solved in a three-dimensional harmonic oscillator basis and a basis of eight major oscillator shells is adopted.

3 Results and discussion

In Fig. 1, the level scheme of candidate AMR bands 4 and 5 in ^{108}In and ^{110}In taken from Ref. [13] is presented. All four bands shown in Fig. 1 are E2 bands with $\Delta I=2$. In ^{108}In, band 4 is assigned to be a negative-parity band with an $I^{\pi}=8^{(-)}$ bandhead directly feeding into the $I^{\pi}=7^{+}$ ground state via a 1861 keV transition; band 5 decays to band 4 through several transitions, which eventually decays to the ground state. Analogously, band 4 in ^{110}In is a negative-parity band with an $I^{\pi}=8^{-}$ bandhead and band 5 is assigned to be a negative-parity band with a $I^{\pi}=9^{(-)}$ bandhead and decays to band 4. Moreover, the similar gamma decay pattern and the excitation energy behaviour for bands 4 and 5 in ^{108}In and ^{110}In in Fig. 1 show evident structural similarity.

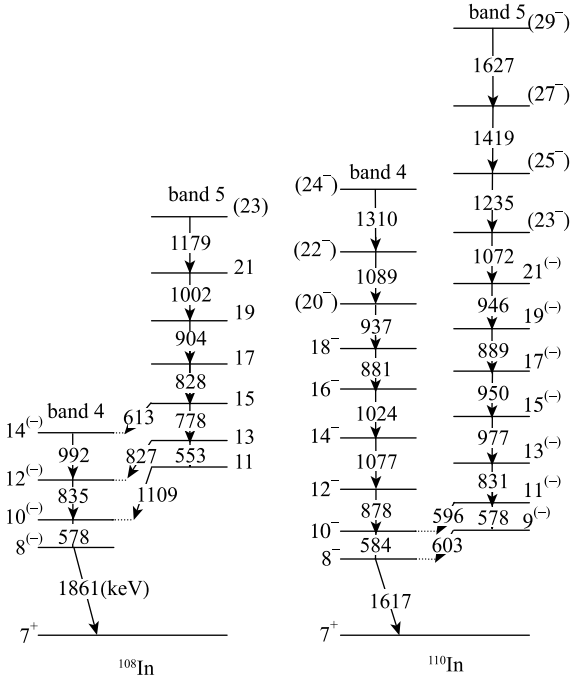

Fig. 1. Level scheme of candidate AMR bands 4 and 5 in ^{108}In and ^{110}In, taken from Ref. [13].

In Ref. [13], bands 4 and 5 in ^{108}In and ^{110}In have been suggested to be candidate AMR bands. Moreover, configurations have been assigned to $\pi g_{9/2}^{-2}d_{5/2}\otimes\nu h_{11/2}$ for band 4 in ^{108}In, $\pi g_{9/2}^{-2}d_{5/2}\otimes\nu h_{11/2}$ and $\pi g_{9/2}^{-2}d_{5/2}\otimes\nu h_{11/2}^{3}$ (after the alignment) for band 4 in ^{110}In, $\pi g_{9/2}^{-2}g_{7/2}\otimes\nu h_{11/2}$ and $\pi g_{9/2}^{-2}g_{7/2}\otimes\nu h_{11/2}^{3}$ (after the alignment) for band 5 both in ^{108}In and ^{110}In. The above configurations are adopted in our TAC-RMF calculations. It should be noted that the tilt angle is 90°, which is obtained self-consistently in the TAC-RMF calculations for all configurations, in accordance with the $\Delta I=2$ character of the bands.

The calculated total energies of these four bands are given in Fig. 2 and compared with the corresponding

data [13]. One observes that the experimental energy increases smoothly with the spin and is well reproduced by the present self-consistent TAC-RMF calculations for all four bands. It should be noted that there are no converged solutions found in the backbend region where the calculated values are missing, due to the level crossing [36].

Spin as a function of rotational frequency for bands 4 and 5 in ^{108}In and ^{110}In obtained from the TAC-RMF calculations in comparison with the corresponding data is shown in Fig. 3. It should be emphasized that for direct comparison with results of the theoretical calculations for $\Delta I = 2$ bands, the experimental rotational frequency can be extracted as in Ref. [34]: $\hbar\omega_{\rm exp} = \frac{1}{2}E_\gamma(I \to I-2)$.

In Fig. 3, it is easy to see that both bands 4 and 5 in ^{110}In show distinct backbend, while there is no backbend observed for band 5 in ^{108}In. In Ref. [13], the backbend has been explained as the rotational alignment of one pair of $h_{11/2}$ neutrons. Based on the suggested configurations, the present TAC-RMF calculations are in general agreement with the experimental $I \sim \omega$ plot and support the configuration assignment, although the calculated spins overestimate the experimental values. For the present TAC-RMF calculations of band 4 in ^{108}In, it can be seen that the calculated spin increases nearly linearly with increasing rotational frequency and reproduces the trend of the experimental data except for an 1–2$\hbar$ overestimate. For band 5 in ^{108}In, the TAC-RMF calculations reproduce the data well before the alignment and overestimate the data by a relatively large amount after the alignment. It is not surprising that the alignment of one pair of $h_{11/2}$ neutrons after the backbend will increase the spin by about 8 $\hbar$. Considering the implicit alignment in band 5 of ^{108}In, strong configuration mixing may exist in the high-spin region, which requires more theoretical studies. For bands 4 and 5 in ^{110}In, the TAC-RMF calculations are in good agreement with the experimental data, although they overestimate them slightly. Taking the pairing correlation into account might improve the result, as discussed in Ref. [37].

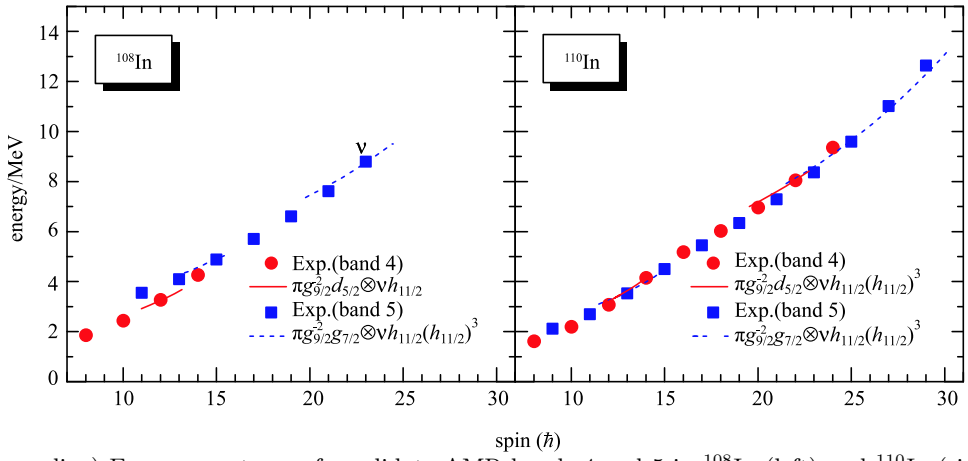

Fig. 2. (color online) Energy spectrum of candidate AMR bands 4 and 5 in ^{108}In (left) and ^{110}In (right) obtained from the TAC-RMF calculations, in comparison with the corresponding data [13].

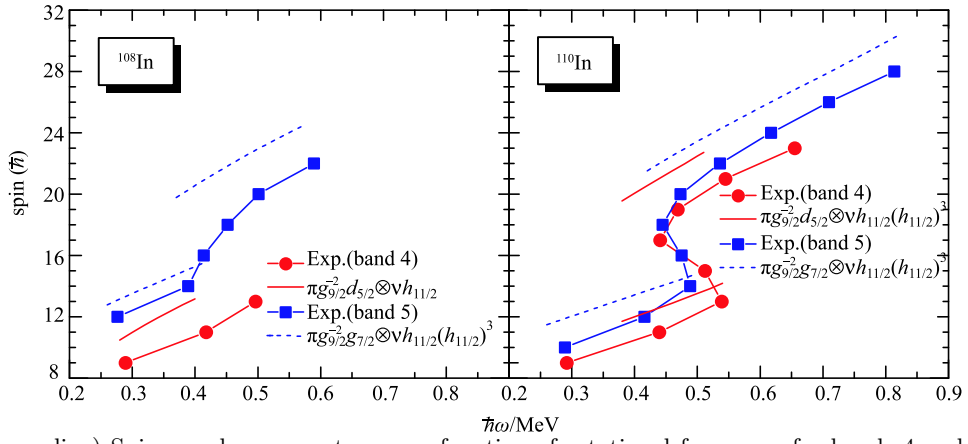

Fig. 3. (color online) Spin angular momentum as a function of rotational frequency for bands 4 and 5 before and after alignment in ^{108}In (left) and ^{110}In (right) obtained from the TAC-RMF calculations in comparison with the corresponding data [13].

To examine the two-shears-like mechanism for the candidate AMR bands in ^{108}In and ^{110}In, the calculated angular momentum vectors contributed from the two-shears-like mechanism, $\boldsymbol{J}_{sh}$, which consists of two proton holes $\pi g_{9/2}^{-2}$, proton particle $\pi d_{5/2}(g_{7/2})$, and neutron particles $\nu h_{11/2}(h_{11/2}^3)$ for the corresponding configurations, are shown in Fig. 4. Taking band 4 of ^{108}In with the configuration $\pi g_{9/2}^{-2} d_{5/2} \otimes \nu h_{11/2}$ as an example, the two $g_{9/2}$ proton holes angular momentum vectors are almost perpendicular to $\boldsymbol{J}_{sh}$ at the beginning ($\hbar\omega =$ 0.28 MeV). Together with the valence particles ($d_{5/2}$ proton and $h_{11/2}$ neutron particles) angular momentum vectors, they form the blades of the two shears. With the increasing rotational frequency ($\hbar\omega$ = 0.40 MeV), the gradual alignment of the proton holes angular momentum vectors toward the particle vectors generates the higher angular momentum while the direction of $\boldsymbol{J}_{sh}$ stays unchanged, which leads to the closing of the two shears simultaneously by moving one blade toward the other. A similar mechanism can also be seen in TAC-RMF calculations with assigned configurations for other candidate AMR bands in ^{108}In and ^{110}In as shown in Fig. 4. It should be noted that here only the angular momentum of orbits for the two-shears-like mechanism, i.e., $\boldsymbol{J}_{sh}$, is involved and the angular momentum apart from the two-shears-like mechanism will be discussed later.

The angular momenta come from the individual nucleons in the self-consistent and microscopic TAC-RMF calculation. In the following, we extract the j_x contributions of nucleon angular momenta in order to investigate the two-shears-like mechanism in a more microscopic way. It should be mentioned that there is no j_z contribution of neutron angular momenta for the present configurations, which is required by the two-shears-like mechanism. The j_x contributions of the two-shears-like orbits (sh), the neutron $(gd)_\nu$ shell, the $Z = 50, N = 50$ core and total angular momenta for the assigned configurations of candidate AMR bands in ^{108}In and ^{110}In are shown in Table 1. The angular momenta of $g_{9/2}$ proton holes, $g_{7/2}(d_{5/2})$ protons and $h_{11/2}$ valence neutrons are the contributions of the two-shears-like mechanism. The remaining neutrons occupying in the $g_{7/2}, d_{5/2}, d_{3/2}$ orbits above $N = 50$ shell are defined as $(gd)_\nu$.

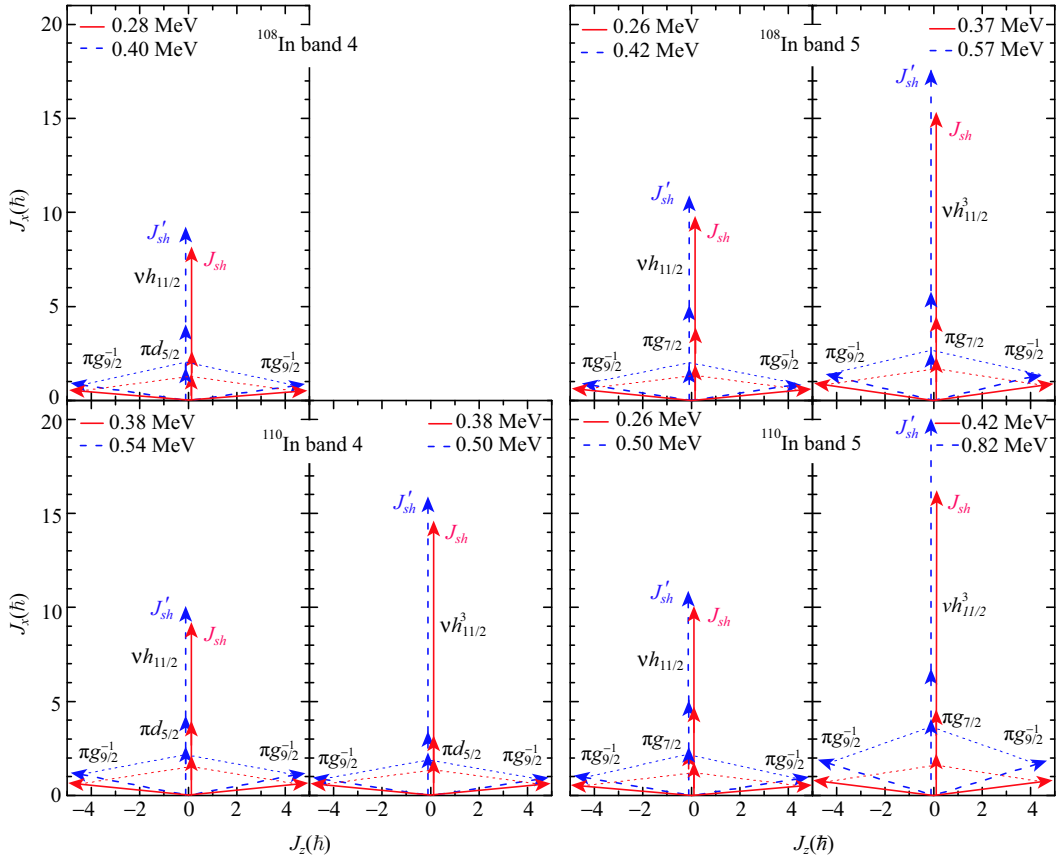

Fig. 4. (color online) Angular momentum vectors of the two-shears-like orbits, $\boldsymbol{J}_{sh}$, contributed from two proton holes $\pi g_{9/2}^{-2}$, proton particle $\pi d_{5/2}(g_{7/2})$, and neutron particles $\nu h_{11/2}(h_{11/2}^3)$ for candidate AMR bands in ^{108}In and ^{110}In calculated with TAC-RMF theory.

Table 1. Calculated angular momenta along the x axis (j_x) in the two-shears-like orbits (sh), the neutron $g_{7/2}, d_{5/2}, d_{3/2}$ orbits above $N = 50$ shell ($(gd)_\nu$), the $Z = 50, N = 50$ core and total angular momenta for the assigned configurations of candidate AMR bands in ^{108}In and ^{110}In.

Conf.		$\pi g_{9/2}^{-2} g_{7/2} \otimes \nu h_{11/2}$			$\pi g_{9/2}^{-2} g_{7/2} \otimes \nu h_{11/2}^{3}$			$\pi g_{9/2}^{-2} d_{5/2} \otimes \nu h_{11/2}$			$\pi g_{9/2}^{-2} d_{5/2} \otimes \nu h_{11/2}^{3}$		
nuclei		$j_x(\hbar)$		Δj_x	$j_x(\hbar)$		Δj_x	$j_x(\hbar)$		Δj_x	$j_x(\hbar)$		Δj_x
^{108}In	$\hbar\omega$/MeV	0.26	0.42		0.37	0.57		0.28	0.40				
	sh	9.2	10.3	1.1	14.8	17.5	2.7	7.5	8.9	1.4			
	$(gd)_\nu$	3.9	5.5	1.6	5.0	6.8	1.8	3.2	4.3	1.1			
	core	0.2	0.3	0.1	0.5	0.6	0.1	0.3	0.5	0.2			
	total	13.3	16.1	2.8	20.3	24.9	4.6	11.0	13.7	2.7			
^{110}In	$\hbar\omega$/MeV	0.26	0.50		0.42	0.82		0.38	0.54		0.38	0.50	
	sh	9.4	10.8	1.4	15.6	19.9	4.3	8.7	9.8	1.1	14.0	15.5	1.5
	$(gd)_\nu$	2.3	4.1	1.8	5.9	10.0	4.1	3.1	4.4	1.3	5.4	6.2	0.8
	core	0.3	0.4	0.1	0.5	1.0	0.5	0.4	0.5	0.1	0.6	1.3	0.7
	total	12.0	15.3	3.3	22.0	30.9	8.9	12.2	14.7	2.5	20.0	23.0	3.0

It is found that the angular momentum contributions from the $Z = 50, N = 50$ core are quite small ($< 1\hbar$), except for the configuration $\pi g_{9/2}^{-2} d_{5/2} \otimes \nu h_{11/2}^{3}$ in ^{110}In. Instead, the contributions to the angular momenta along the x axis originate mainly from the two-shears-like orbits, and the $(gd)_\nu$ shell contribution is relatively small. For example, for the assigned configuration $\pi g_{9/2}^{-2} g_{7/2} \otimes \nu h_{11/2}$ of candidate band 4 in ^{108}In, two-shears-like orbits contribute $9.2 \sim 10.2\ \hbar$, 8 neutrons in the $(gd)_\nu$ shell contribute $4.2 \sim 5.2\ \hbar$ and the core contributes $0.3 \sim 0.4\ \hbar$. However, with the increasing rotational frequency, both sh and $(gd)_\nu$ contribute with a comparable increment to the angular momentum, $0.7\ \hbar$ and $1.0\ \hbar$, respectively. Although the two-shears-like mechanism is important, the remaining neutrons in the $(gd)_\nu$ shell are still making large contributions. As the pairing correlations always tend to hinder the angular momentum alignment of nucleons, it is expected that the inclusion of the pairing correlations will decrease the calculated values of the total angular momentum, and give a better description of the $I \sim \omega$ relations in Fig. 3.

Typical characteristics of AMR include weak E2 transitions, reflecting the small deformation of the core, as well as a decreasing tendency of the reduced transition probability B(E2) values with increasing spin, which results in large ratios of the dynamic moments of inertia $\mathfrak{J}^{(2)}$ to the B(E2) values. In Fig. 5, B(E2) and $\mathfrak{J}^{(2)}/B$(E2) as a function of the spin for bands 4 and 5 in ^{108}In and ^{110}In obtained from the TAC-RMF calculations are shown in comparison with the data.

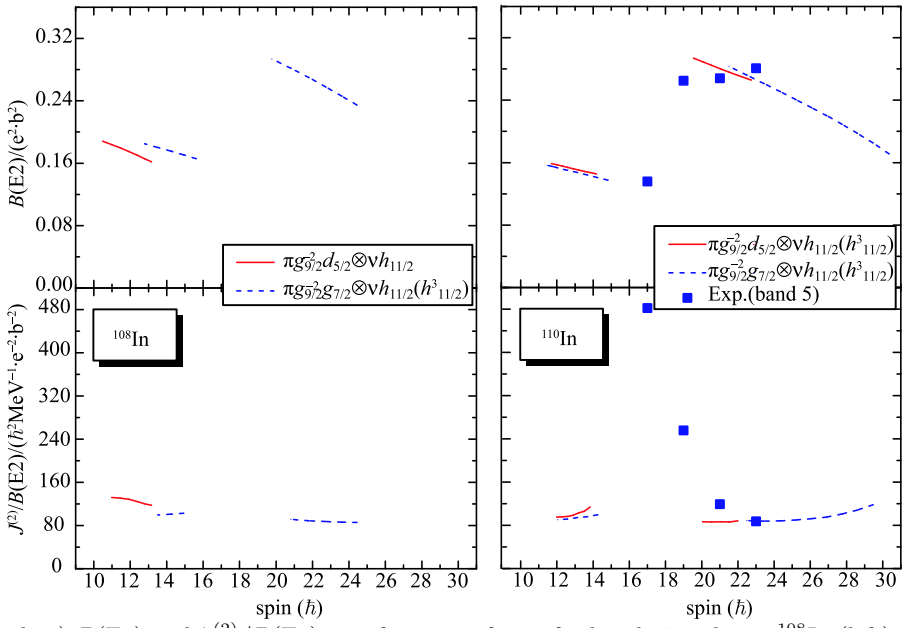

Fig. 5. (color online) B(E2) and $\mathfrak{J}^{(2)}/B$(E2) as a function of spin for bands 4 and 5 in ^{108}In (left) and ^{110}In (right) obtained from the TAC-RMF calculations in comparison with the corresponding data [13].

It can be seen that the B(E2) values show smooth decreasing tendencies with increasing rotational frequencies in the calculations for all four bands and are all lower than $0.20\,\mathrm{e}^2\cdot\mathrm{b}^2$ before the alignment or $0.30\,\mathrm{e}^2\cdot\mathrm{b}^2$ after the alignment, which are relatively small values. This means that the E2 transitions are relatively weak. Besides, the $\mathfrak{J}^{(2)}/B$(E2) ratios are around $100\,\hbar^2\mathrm{MeV}^{-1}\cdot\mathrm{e}^{-2}\cdot\mathrm{b}^{-2}$ or more, which are much higher than $10\,\hbar^2\mathrm{MeV}^{-1}\cdot\mathrm{e}^{-2}\cdot\mathrm{b}^{-2}$ for well deformed heavy nuclei and $5\,\hbar^2\mathrm{MeV}^{-1}\cdot\mathrm{e}^{-2}\cdot\mathrm{b}^{-2}$ for superdeformed nuclei [1]. This result is consistent with the expectation for a two-shears-like mechanism.

Experimental B(E2) values and $\mathfrak{J}^{(2)}/B$(E2) ratios for band 5 in ^{110}In obtained from Ref. [13] are given in the right panel of Fig. 5. It is easy to see that the experimental B(E2) values before and after alignment in band 5 of ^{110}In are approximately $0.14\,\mathrm{e}^2\cdot\mathrm{b}^2$ and $0.265\,\mathrm{e}^2\cdot\mathrm{b}^2$, respectively, in agreement with the present TAC-RMF calculations for the configuration $\pi g_{9/2}^{-2}g_{7/2}\otimes\nu h_{11/2}^3$ before alignment and the configuration $\pi g_{9/2}^{-2}g_{7/2}\otimes\nu h_{11/2}^3$ after alignment as shown in Fig. 5, which further indicates that the present calculations are reasonable. A similar conclusion can also be obtained for the experimental $\mathfrak{J}^{(2)}/B$(E2). Moreover, the available experimental B(E2) and $\mathfrak{J}^{(2)}/B$(E2) for band 5 in ^{110}In are in numerical agreement with the confirmed AMR bands in ^{105}Cd [4],^{106}Cd [5], ^{107}Cd [6], ^{108}Cd [7, 8], ^{110}Cd [9], ^{101}Pd [10] and ^{104}Pd [11].

It should be noted that the experimental $\mathfrak{J}^{(2)}/B$(E2) at $I=16\,\hbar$ is very large, as it is in the alignment region. However, the available experimental B(E2) does not exhibit a decreasing behavior. Similar behavior has also been observed in the higher part of the $\nu h_{11/2}$ band in ^{101}Pd [10] and the negative-parity yrast sequence of ^{109}Cd [36, 38, 39]. Besides the two-shears-like mechanism, the collective motion from the core may also provide a large contribution. However, more lifetime measurements and further theoretical explanations need to be demonstrated for a more conclusive interpretation.

The decrease of the B(E2) values can be understood by the changes in nuclear deformation. Deformation parameters β and γ as a function of spin for bands 4 and 5 in ^{108}In and ^{110}In obtained from the TAC-RMF calculations are shown in Fig. 6. In comparison with Fig. 5, it is found that the decreasing tendencies of β and B(E2) with increasing spin are similar, which could be interpreted as the nuclear deformation reflecting the charge distribution in the nuclei, which has effect on B(E2). It can be seen in Fig. 6 that β values are lower than 0.25 but higher than 0.18 for all bands, which means that ^{108}In and ^{110}In are not well-deformed nuclei. The calculated γ values increase with increasing rotational frequency for all bands except for band 4 in ^{110}In.

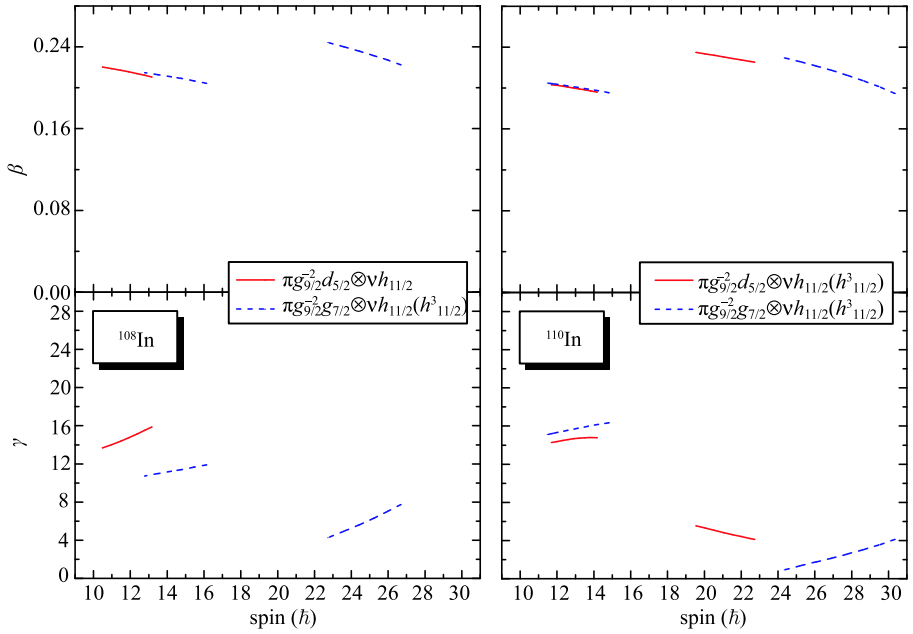

Fig. 6. (color online) Deformation parameters β (upper panel) and γ (lower panel) as a function of spin for bands 4 and 5 in ^{108}In (left) and ^{110}In (right) obtained from the TAC-RMF calculations.

4 Summary

In this paper, based on the tilted axis cranking relativistic mean field theory within point-coupling interaction PC-PK1, the candidate AMR bands in ^{108,110}In have been studied. Based on the previous suggested configurations, TAC-RMF calculations reproduce the experimental energy spectrum well and are in agreement with

the experimental $I \sim \omega$ plot, although the calculated spins overestimate the experimental values. In addition, the two-shears-like mechanism in candidate AMR bands has been clearly illustrated and the contributions from the two-shears-like orbits, the neutron (gd) orbits above $Z = 50$ shell and the $Z = 50$, $N = 50$ core have been investigated microscopically. The predicted B(E2), dynamic moment of inertia $\mathfrak{J}^{(2)}$, deformation parameters β and γ, and $\mathfrak{J}^{(2)}/B$(E2) ratios in TAC-RMF calculations have been discussed and the characteristic features of AMR for the bands before and after alignment have been shown. However, more investigations such as lifetime measurements will be useful to make a conclusive interpretation in the future.

References

1 S. Frauendorf, Rev. Mod. Phys., **73**: 463 (2001)
2 J. Meng et al, Front. Phys., **8**: 55 (2013)
3 J. Meng, S. Q. Zhang, and P. W. Zhao, Novel rotational excitations, in *Relativistic Density Functional for Nuclear Structure*, Edited by Jie Meng Singapore: World Scientific, (2016)
4 D. Choudhury et al, Phys. Rev. C, **82**: 061308 (2010)
5 A. J. Simons et al, Phys. Rev. Lett., **91**: 162501 (2003)
6 D. Choudhury et al, Phys. Rev. C, **87**: 034304 (2013)
7 A. J. Simons et al, Phys. Rev. C, **72**: 024318 (2005)
8 P. Datta et al, Phys. Rev. C, **71**: 041305 (2005)
9 S. Roy et al, Phys. Lett. B, **694**: 322 (2011)
10 M. Sugawara et al, Phys. Rev. C, **86**: 034326 (2012)
11 N. Rather et al, Phys. Rev. C, **89**: 061303 (2014)
12 S. Zhu et al, Phys. Rev. C, **64**: 041302 (2001)
13 C. J. Chiara et al, Phys. Rev. C, **64**: 054314 (2001)
14 X. W. Li et al, Phys. Rev. C, **86**: 057305 (2012)
15 M. Sugawara et al, Phys. Rev. C, **79**: 064321 (2009)
16 B. D. Serot and J. D. Walecka, Adv. Nucl. Phys., **16**: 1 (1986)
17 B. A. Nikolaus, T. Hoch, and D. G. Madland, Phys. Rev. C, **46**: 1757 (1992)
18 W. H. Long, N. Van Giai, and J. Meng, Phys. Lett. B, **640**: 150 (2006)
19 P. G. Reinhard, Rep. Prog. Phys., **52**: 439 (1989)
20 P. Ring, Prog. Part. Nucl. Phys., **37**: 193 (1996)
21 D. Vretenar et al, Phys. Rep., **409**: 101 (2005)
22 J. Meng et al, Prog. Part. Nucl. Phys., **57**: 470 (2006)
23 P. W. Zhao et al, Phys. Rev. C, **85**: 054310 (2012)
24 J. Peng and P. W. Zhao, Phys. Rev. C, **91**: 044329 (2015)
25 D. Steppenbeck et al, Phys. Rev. C, **85**: 044316 (2012)
26 P. W. Zhao et al, Phys. Lett. B, **699**: 181 (2011)
27 H. Madokoro, J. Meng, M. Matsuzaki, and S. Yamaji, Phys. Rev. C, **62**: 061301(R) (2000)
28 Y. Zheng et al, J. Phys. G, **42**: 085108 (2015)
29 J. Li et al, Phys. Rev. C, **88**: 014317 (2013)
30 K. Y. Ma et al, Eur. Phys. J. A, **48**: 82 (2012)
31 C. B. Li et al, Nucl. Phys. A, **892**: 34 (2012)
32 J. Peng, J. Meng, P. Ring, and S. Q. Zhang, Phys. Rev. C, **78**: 024313 (2008)
33 L. F. Yu et al, Phys. Rev. C, **85**: 024318 (2012)
34 S. Frauendorf and J. Meng, Z. Phys. A, **356**: 263 (1996)
35 P. W. Zhao, Z. P. Li, J. M. Yao, and J. Meng, Phys. Rev. C, **82**: 054319 (2010)
36 P. Zhang, B. Qi, and S. Y. Wang, Phys. Rev. C, **89**: 047302 (2014)
37 P. W. Zhao, S. Q. Zhang, and J. Meng, Phys. Rev. C, **92**: 034319 (2015)
38 C. J. Chiara et al, Phys. Rev. C, **61**: 034318 (2000)
39 S. Roy and S. Chattopadhyay, Phys. Rev. C, **83**: 024305 (2011)